

Resolving Electronic Transitions in Synthetic Fluorescent Protein Chromophores by Magnetic Circular Dichroism

Petr Štěpánek,^[b] Thomas Y. Cowie,^[a] Martin Šafařík,^[a] Jaroslav Šebestík,^[a] Radek Pohl,^[a] and Petr Bouř^{✉*}^[a]

The detailed electronic structures of fluorescent chromophores are important for their use in imaging of living cells. A series of green fluorescent protein chromophore derivatives is examined by magnetic circular dichroism (MCD) spectroscopy, which allows the resolution of more bands than plain absorption and fluorescence. Observed spectral patterns are rationalized with the aid of time-dependent density functional theory (TDDFT) computations and the sum-over-state (SOS) formalism, which also reveals a significant dependence of MCD intensities

on chromophore conformation. The combination of organic and theoretical chemistry with spectroscopic techniques also appears useful in the rational design of fluorescence labels and understanding of the chromophore's properties. For example, the absorption threshold can be heavily affected by substitution on the phenyl ring but not much on the five-member ring, and methoxy groups can be used to further tune the electronic levels.

1. Introduction

Fluorescent proteins (FPs) are fantastic tools to visualize the cellular structure and processes in living organisms. They have been extensively studied and have recently been used to directly influence metabolic pathways.^[1] More than a decade after discovery of the first green FP^[2] the importance of the structure to the chromophore has been recognized.^[3] Since then, numerous FP variants have been found, differing in both the protein and chromophore components.^[4] Although the structure of the chromophore varies,^[4,5] a five-member imidazolinone ring must be present as a core motif. The imidazolinone connected through the $-C=$ bridge to another residue with conjugated electrons thus seems to be crucial for all fluorescence applications.

Fluorescence properties are determined not only by the chemical structure of the chromophore but also by the environmental conditions of the protein including pH. Mutations to the green FP have created mutant strains to provide varying emission wavelengths, enhanced absorption cross-sections and protein folds.^[1,5] Due to the complexity in identifying specific modifications it is currently difficult to design fluorescent labels of specific properties by only using means of synthetic and computational chemistry.

In the present study we test how chemical modification can influence spectral properties and the electronic structure of a series of FP chromophore derivatives, and determine how reproducible these changes are by advanced quantum chemical computations. The fluorescence, absorption and magnetic circular dichroism (MCD) spectra of FP chromophore derivatives were measured and compared with predictions based on the time-dependent density functional theory (TDDFT). The absorption and MCD spectra are known to be closely related to the fluorescent properties.^[4,6]

MCD spectroscopy^[7] has been useful in assigning and resolving the electronic transitions of a wide range of organic and inorganic molecules. MCD is a differential absorption of the left- and right-circularly polarized light in a permanent magnetic field parallel to the light propagation. It can be both negative and positive and provides additional information on the absorption and fluorescence properties. Planar molecules with conjugated electrons do not exhibit natural circular dichroism but may still have a large MCD signal. As of writing, MCD spectroscopy has not been applied to the examinations of FP chromophores yet.

Modern quantum MCD theory appeared in the 1970s,^[8] but only the recent implementations within DFT^[9] are applicable to sizable systems. The present study thus also documents how theoretical simulations significantly enhance the MCD potential to provide insights into structural and chemical problems.^[9,10]

Several computational approaches have been applied to understand the FP chromophore's excited electronic states in the past.^[11] Recently, the method for reduced virtual-space approach for approximating second-order coupled clusters (RVSCC2)^[12] were applied to investigate changes in green FP chromophore at different ionic states.^[13] The importance of the polarization effect for excitation energies were emphasized in

[a] T. Y. Cowie, Dr. M. Šafařík, Dr. J. Šebestík, Dr. R. Pohl, Prof. P. Bouř
Institute of Organic Chemistry and Biochemistry, AS CR
Flemingovo náměstí 2, 166 10 Prague (Czech Republic)
E-mail: bour@uochb.cas.cz

[b] P. Štěpánek
NMR Research Group
Faculty of Science, University of Oulu
PO Box 3000, 90014 Oulu (Finland)

Supporting Information for this article can be found under <http://dx.doi.org/10.1002/cphc.201600313>.

a complex study using time-dependent density functional theory (TDDFT), multiconfigurational perturbation theory (CASPT2), and quantum Monte Carlo (QMC) methods.^[14] The polarization effect was confirmed by works which combined TDDFT with polarizable embedding (PE) of the FP chromophore.^[15] The PE approximation was thoroughly tested and found very suitable for fast estimations of the environmental effects on the chromophore.^[16] Effects of chemical modifications to the green FP chromophore were studied using TDDFT and molecular dynamics (MD),^[17] and intermolecular charge transfer in yellow FP was estimated using TDDFT and CC2 approaches.^[18] Ground- and excited-states vibrations and dielectric response to photoexcitation were estimated at the complete active space self-consistent field (CASSCF) level.^[19] Extensive benchmarking of the quantum chemical methods was done on several simplified FP chromophores.^[20]

We use TDDFT to calculate excited electronic states of a series of synthetic FP chromophore derivatives (Figure 1); the method provides reasonably accurate results with acceptable computational cost.^[11,20a,b,21] The sum-over-state methodology (SOS)^[9 h,22] is used for simulations of MCD intensities, which

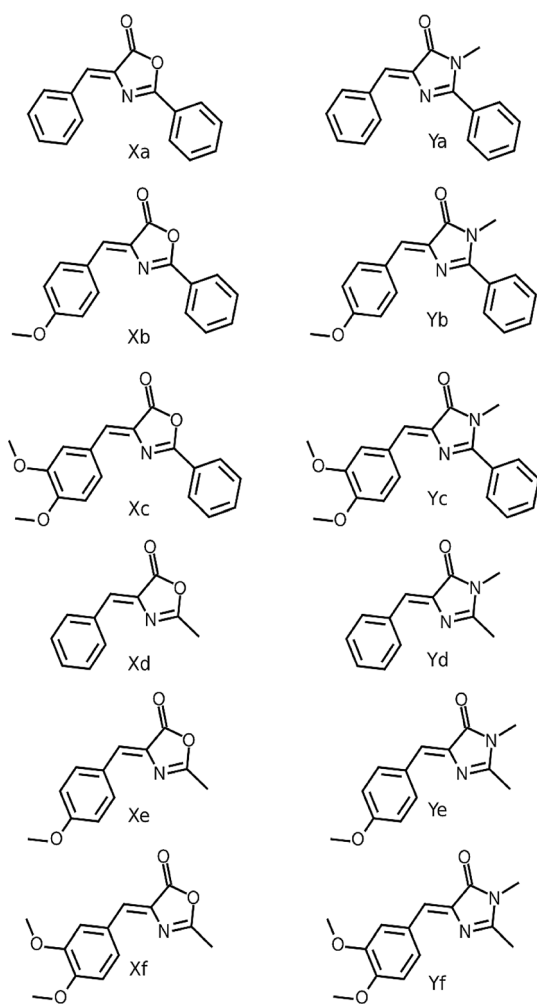


Figure 1. Investigated compounds, precursors (Xn) and variously substituted native FP chromophores (Yn).

has been successfully applied for fullerene derivatives.^[10b,23] We find it efficient with respect to the required computer time, although efficient implementations of other procedures, such as the complex polarization propagator (CPP) methods,^[9b] have also been reported and tested.^[24] As shown below the SOS calculations reproduce the main trends observed in the experimental spectra.

2. Results and Discussion

Experimental and calculated absorption spectra of the chromophore derivatives are plotted in Figure 2. For Ya, only the calculated spectra are shown as the synthesis was not successful.

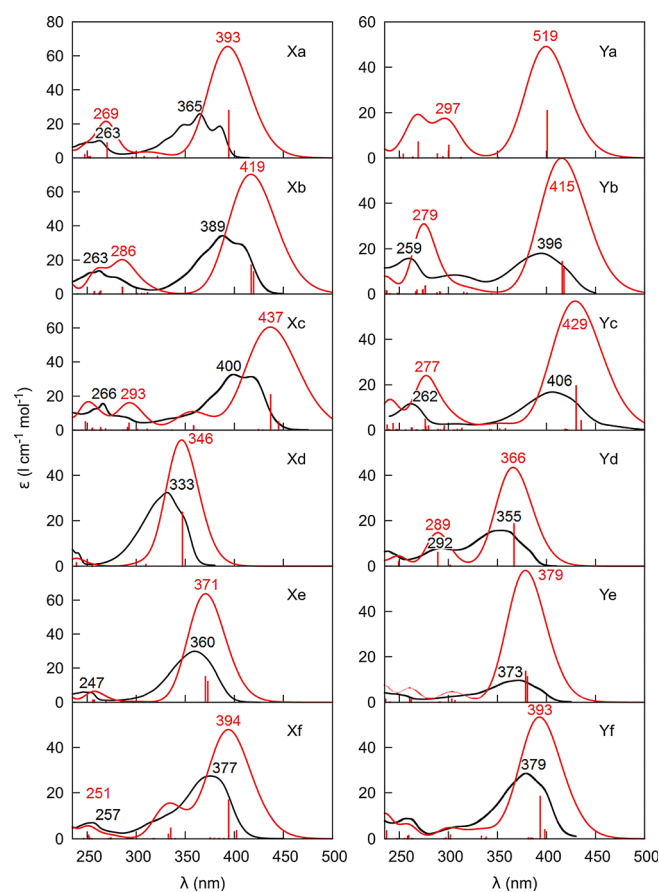


Figure 2. Experimental (black) and calculated (red, obtained as Boltzmann averages of individual conformers; absorption lines in arbitrary units are indicated as well) absorption spectra of model chromophores.

The measured wavenumber range was limited by a strong absorption of the chloroform solvent below ~ 240 nm. The spectra confirm the stability of the electronic structure of the FP chromophore skeleton; they are similar with a dominant high-wavelength absorption band that is separated by about 70 nm (~ 0.6 eV) from the others. The experimental spectral patterns are consistent with previous observations on other FP chromophore compounds.^[11,17,20c,d,25] In the experiment, the broad longest-wavelength bands are often nearly split or exhibit fine

structure, most probably due to conformer equilibria and electronic–vibrational interactions.^[19a,26]

Within the Y-series the least substituted **Yd** derivative exhibits the lowest-wavelength absorption threshold (~400 nm) and the strongest experimental absorption at 355 nm. The methoxy substitution in **Ye** has caused a red-shift of 18 nm and with the dimethoxy derivative **Yf** the maximum has been shifted by 6 nm further right to 379 nm. Replacement of the methyl group by phenyl on the imidazolinone ring (**Yd**→**Yb, Yc**) causes much larger shifts of about 50 nm from the maximum. The calculations reveal that introduction of the second benzene ring in **Ya–Yb** results in additional transitions in the lower-wavelength region (240–350 nm) without a significant change in the overall absorption. The **Yd–Yf** derivatives have three transitions within 240–500 nm only. Computed absorption intensities appear mostly larger than the observed ones, by ~20–200%, and the transitions wavelength are systematically higher, otherwise the computation reproduces the main experimental trends. Note that accuracy of the experimental intensity may vary as well because of limited solubility and gradual evaporation of the chloroform solvent during the relatively long MCD accumulation times.

In the precursor series (**Xa–Xf**) the same absorption pattern, namely, a large relatively separate high-wavelength band, and less intense transitions below 350 nm, is conserved. The nitrogen–oxygen exchange in the imidazolinone ring (**Yd**→**Xd**) causes a large absorption increase (by about 50%) and a blue-shift of the principle band from 355 to 360 nm (~0.2 eV) in experiment, which is well reproduced by the calculations. Further substitutions by the phenyl and methoxy groups cause similar effects as for the nitrogen derivatives **Ya–Yf**.

Corresponding calculated and experimental MCD spectra are plotted in Figure 3. As expected MCD intensities are more variable than the absorption because they are more sensitive to differences in the geometry and electronic structure.^[9c,9 g,10b,27] However, a general pattern can be observed for all compounds, too. Typical is a negative MCD peak at the longest-wavelength region (>300 nm), and stronger multiple bands around 250 nm. Experimental MCD spectra of the lowest-energy transition are hampered by a large noise caused by small CD/absorption ratio. This highest-wavelength MCD signal is in general more developed in the oxazolones **Xa–Xf**; the **Xe** derivative provides the largest MCD intensity of $-0.25 \text{ L cm}^{-1} \text{ mol}^{-1} \text{ T}^{-1}$ at around 356 nm.

The computations allow us to assign most of the observed MCD spectral features to particular electronic transitions although there are several inconsistencies explicable by the limited accuracy of the simulations. In **Xd**, however, the positive experimental signal at 333 nm is not reproduced at all, and the correspondence between the simulated and MCD intensities within 250–300 nm for **Yb** and **Yc** is not obvious.

To investigate more limitations of the theoretical approach, in Figure S1 MCD spectra are plotted as recalculated by alternate SOS-gradient method.^[9h] This, however, provided similar intensities to the default SOS-length formula [Eq. (1) in the Experimental Section]. Larger discrepancies appeared between the B3LYP^[28] and M062X^[29] functional (Figure S2A). The latter is

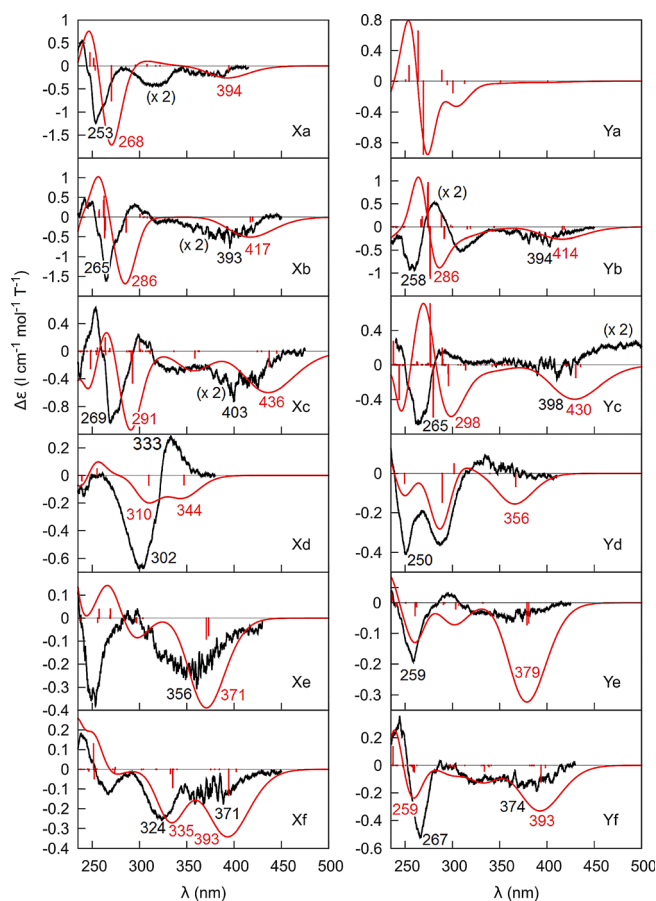


Figure 3. Experimental (black) and calculated (red) MCD spectra of studied chromophores, corresponding to the absorption in Figure 2. Experimental intensities of **Xa**, **Xb**, **Xc**, **Yb** and **Yc** were multiplied by two.

applicable to a wider class of compounds than the more common B3LYP.^[29] However, for our compounds, none provides convincingly better agreement with the experiment than the other. The B3LYP band wavelengths are slightly higher and the M062X ones lower than in experiment. Another long-range corrected functional, CAM-B3LYP,^[30] provided similar results as M062X, and the pure GGA B86^[31] functional gave rather unrealistic spectra (Figure 2 SB). Such a limited accuracy of DFT is consistent with previous works,^[17,20b,21] and future improvement may be difficult because of the complex interplay between the functional parameterization, solvent models, vibrational effects, and so forth.^[32]

The dependence of the MCD spectra on the conformation is documented for all stable conformers of **Xc** (listed in Table S1) in Figure 4. Such sensitivity is rather surprising. For example, in our previous study of aromatic aminoacids the effect of the conformation on MCD intensities was rather limited.^[33] For the FP chromophores, however, relevant excitations involve electron rearrangement across the rotating bonds and proper conformational weighting is needed to reproduce the experimental data. The largest conformation-related changes occur within 200–300 nm, while the highest-wavelength band (~420 nm) is negative for all twelve conformers.

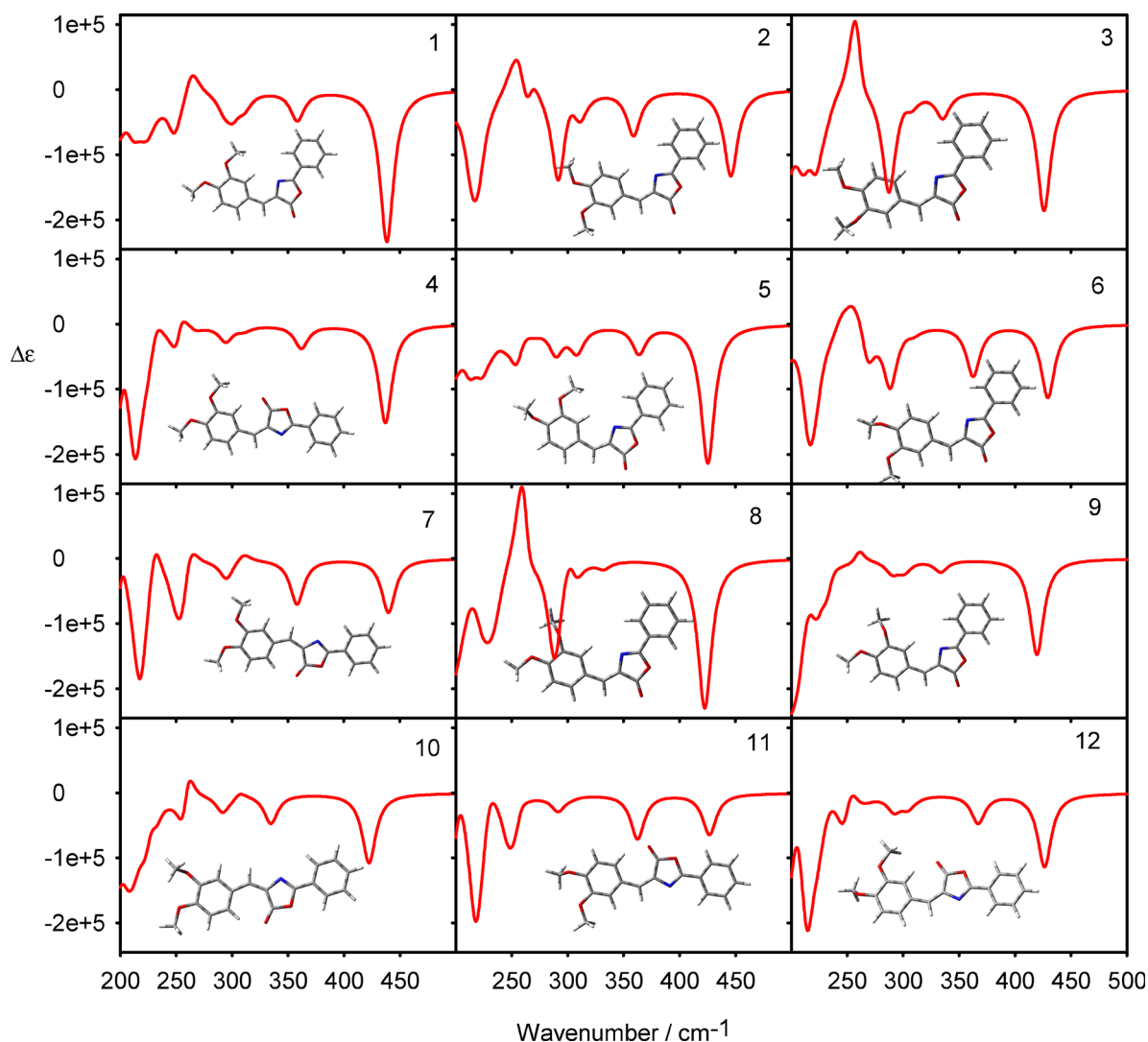


Figure 4. Calculated MCD spectra of stable Xc conformers.

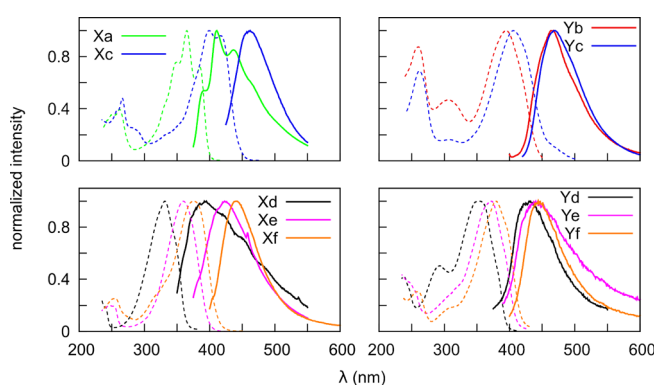


Figure 5. Experimental fluorescence (solid line) and absorption (dashed) spectra, normalized to the maximum = 1.

Most compounds also exhibited measurable fluorescence and the spectra are plotted together with the normalized absorption in Figure 5. Energies of the absorption and fluores-

Table 1. Energies of the lowest-energy absorption (calculated, $E_{A,cal}$ and experimental, $E_{A,exp}$) and fluorescence bands ($E_{F,cal}$, $E_{F,exp}$), in eV.								
	$E_{A,cal}$	$E_{A,exp}$	$E_{F,cal}$	$E_{F,exp}$		$E_{S,cal}$	$E_{S,exp}$	
Xa	3.14	3.40	2.67	3.02	Ya	3.09	–	2.47
Xb	2.97	3.20	2.59	–	Yb	2.98	3.15	2.42
Xc	2.81	3.11	2.53	2.68	Yc	2.96	3.05	2.41
Xd	3.57	3.75	3.07	3.15	Yd	3.38	3.49	2.82
Xe	3.35	3.44	3.01	2.92	Ye	3.27	3.33	2.82
Xf	3.18	3.31	2.83	2.81	Yf	3.25	3.27	2.80

cence maxima are compared to the computations in Table 1. As expected, the experimental lowest-energy absorption and fluorescence peak positions differ by the relaxation energy, about 0.4–0.6 eV, which is well reproduced by the calculations. The relaxation of the first excited singlet state leads to minor changes in the chromophore geometries, which can be seen in Figure S3. However, fluorescence intensity/efficiency significantly varied among the derivatives, analysis of which goes

Table 2. Calculated wavelengths and principal orbital contributions to the lowest-energy transitions in lowest-energy <i>cis</i> and <i>trans</i> conformers (cf. angle φ_{17} , Table S1) of Xd and Yd .			
λ [nm] <i>cis</i> - Xd		λ [nm] <i>cis</i> - Yd	
347	HOMO→LUMO (100%)	367	HOMO→LUMO (98%)
310	HOMO-1→LUMO (94%)	302	HOMO-1→LUMO (91%)
		289	HOMO-3→LUMO (93%)
<i>trans</i> - Xd		<i>trans</i> - Yd	
352	HOMO→LUMO (100%)	371	HOMO→LUMO (97%)
314	HOMO-1→LUMO (94%)	304	HOMO-1→LUMO (91%)
		288	HOMO-3→LUMO (94%)

beyond the scope of the present study. The variations are consistent with the strong dependence of the FP fluorescence on the local environment of the chromophore.^[4]

The transition assignment is rather straightforward and analogous for all compounds. As an example the lowest-energy transitions in **Xd** and **Yd** is summarized in Table 2. Also the HOMO and LUMO orbitals are in different compounds remarkably similar; in Figure 6 the orbitals are plotted for **Xc**–**Xe** only. The lowest-energy transitions are thus almost exclusively caused by the HOMO→LUMO excitation, with the second lowest transition being predominantly HOMO-1→LUMO, and the character of the transitions is not significantly changed by the conformation of the substituents. Perhaps this simplicity and stability of the electronic structure contributes to the universal applicability of the fluorescent labels based on the FP chromophores.

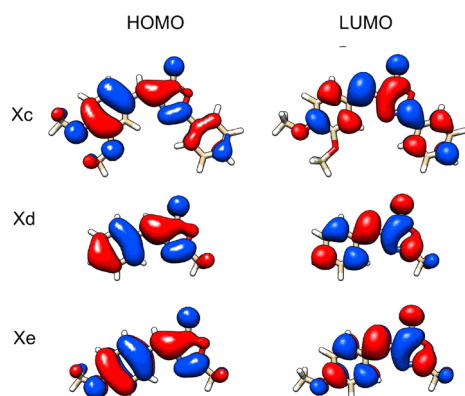


Figure 6. Frontier orbitals of **Xc**–**Xe**.

3. Conclusions

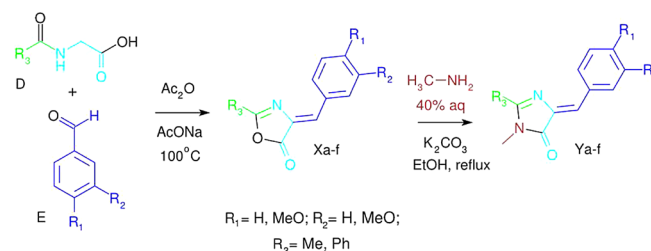
The synthetic series of derivatives of the fluorescent protein chromophore helped us to better understand the relation between the structure and electronic properties, important for rational design of fluorescent labels. MCD spectroscopy proved useful both as a tool for chromophore discrimination and assignment of observed electronic transitions. Surprising was also the dependence of the MCD pattern on the conformation, possibly usable in future structural studies. The TDDFT/SOS

computations reproduced the main trends in the excitation electronic energies, absorption, and MCD spectral intensities that were observed experimentally.

Experimental Section

Organic Synthesis

The synthesis was based on strategy of Kojima et al.^[25] using oxazolones precursors (Scheme 1). The precursors containing oxygen in the five-membered ring were converted to FP chromophores using condensation with methylamine. Purity of the products was controlled using HPLC, mass spectroscopy and NMR. Synthetic details can be found in the Supporting Information.



Scheme 1. General synthesis scheme.

Spectra Measurement

MCD and absorption spectra were acquired on a Jasco J-815 (Japan) spectrometer equipped with 1.5 T permanent magnet. The samples were dissolved in CHCl_3 freshly purified by alumina and measured in quartz cell of 1 mm optical path, at room temperature (295 K), using a scanning speed of 5 nm min^{-1} , and concentrations within $0.075\text{--}1.4 \text{ mg mL}^{-1}$ according to optimal absorption with respect to MCD measurement. Fluorescence spectra were measured on a Horiba Fluoromax-4 spectrometer for solutions in ethanol; chloroform as a solvent provided negligible fluorescence intensities only. Unlike the intensities, fluorescence peak positions measured in ethanol and chloroform are expected to be similar.^[34] Excitation wavelengths listed in the Supporting Information were chosen to maximize the signal.

Spectra Modeling

Equilibrium geometries and excited electronic states were obtained using the Gaussian 09 program.^[35] The standard $6\text{-}311++\text{G}^{**}$

basis set and Gaussian version (CPCM) of the conductor-like solvent model (COSMO)^[36] were used, previously giving reasonable results for similar system.^[33] Geometry optimizations were performed at the B3LYP^[28]/6-311 + G** level of approximation. Excited states were calculated using time-dependent DFT (TDDFT)^[37] and the B3LYP functional. In some cases M062X BP86 and CAM-B3LYP functionals were tried as well. 400 lowest-energy excited states obtained by Gaussian were used for sum-over-states (SOS)^[9 h,22] simulations of MCD intensities using our own software (“GUVUDE”). The origin-independent SOS expression^[22] was used by default where the Faraday “B-term” determining the MCD intensities for an $n \rightarrow j$ transition is equal to [Eq. (1)]

$$B = \frac{1}{2} \left\{ \sum_{k \neq n} \left[\frac{\langle k | \sum_{i=1}^{N_e} \mathbf{r}_i \times \nabla_i | n \rangle}{E_{kn}} + \frac{1}{2N_e} \left(\sum_{l \neq n} \frac{\boldsymbol{\mu}_{kl} \times \nabla_{ln}}{E_{ln}} + \sum_{l \neq k} \frac{\boldsymbol{\mu}_{ln} \times \nabla_{kl}}{E_{kl}} \right) \right] \cdot \boldsymbol{\mu}_{nj} \times \boldsymbol{\mu}_{jk} + \sum_{k \neq j} \left[\frac{\langle j | \sum_{i=1}^{N_e} \mathbf{r}_i \times \nabla_i | k \rangle}{E_{kj}} + \frac{1}{2N_e} \left(\sum_{l \neq k} \frac{\boldsymbol{\mu}_{jl} \times \nabla_{lk}}{E_{lk}} + \sum_{l \neq j} \frac{\boldsymbol{\mu}_{lk} \times \nabla_{jl}}{E_{jl}} \right) \right] \cdot \boldsymbol{\mu}_{nj} \times \boldsymbol{\mu}_{kn} \right\} \quad (1)$$

where n denotes the ground state, j , k , and l are excited states modeled by the TDDFT single excitations, i is used for the electron index, N_e is the number of electrons, \mathbf{r}_i is position of an electron i , $\boldsymbol{\mu}_{ab} = \langle a | \boldsymbol{\mu} | b \rangle$ denotes electric dipole matrix element, $E_{ab} = E_a - E_b$ is the difference in excitation (not orbital) energies. The apostrophe means that the energy in the denominator was replaced by a “degeneracy-resistant” expression, as shown by Equation (2):

$$\frac{1}{E'_{ab}} = \frac{E_{ab}}{E_{ab}^2 + \Gamma^2} \quad (2)$$

where $\Gamma = 0.02$ hartree. Resultant absorption and MCD spectra were simulated as a Boltzmann average of individual conformers, using Lorentzian bandwidth of full width at half height of 0.2 eV. In Figure 4 and S2B 15 nm width was used to emphasize individual transitions. Fluorescence energies were computed as the vertical excitation energies for the lowest-energy conformers optimized in the first electronic excited state.

Acknowledgements

The work was supported by the Grant Agency of the Czech Republic (grant numbers 13-03978S and 16-059355). We thank Dr. D. Padula for the help with the calculations.

Keywords: density functional calculations · fluorescence protein chromophores · magnetic circular dichroism · organic synthesis · spectral simulations

- [1] C. Brieke, F. Rohrbach, A. Gottschalk, G. Mayer, A. Heckel, *Angew. Chem. Int. Ed.* **2012**, *51*, 8446–8476; *Angew. Chem.* **2012**, *124*, 8572–8604.
- [2] O. Shimomura, F. H. Johnson, Y. Saiga, *J. Cell. Comp. Physiol.* **1962**, *59*, 223–239.
- [3] O. Shimomura, *FEBS Lett.* **1979**, *104*, 220–222.
- [4] D. M. Chudakov, M. V. Matz, S. Lukyanov, K. A. Lukyanov, *Physiol. Rev.* **2010**, *90*, 1103–1163.
- [5] a) A. Follenius-Wundt, M. Bourotte, M. Schmitt, F. Ilyce, L. Hans, J. J. Bourguignon, J. Haiech, C. Pigault, *Biophys. J.* **2003**, *85*, 1839–1850; b) A. B. Cubitt, R. Heim, S. R. Adams, A. E. Boyd, L. A. Gross, R. Y. Tsien, *Trends Biochem. Sci.* **1995**, *20*, 448–455; c) B. P. Cormack, R. H. Valdivia, S. Falkow, *Gene* **1996**, *173*, 33–38; d) S. J. Remington, *Methods Enzymol.* **2000**, *305*, 196–211.

- [6] M. F. Garcia-Parajo, G. M. J. Segers-Nolten, J. A. Veerman, J. Greve, N. F. van Hulst, *Proc. Natl. Acad. Sci. USA* **2000**, *97*, 7237–7242.
- [7] W. R. Mason, *A Practical Guide to Magnetic Circular Dichroism Spectroscopy*, Wiley-Interscience, New York, **2007**.
- [8] a) P. J. Stephens, *J. Chem. Phys.* **1970**, *52*, 3489–3516; b) P. J. Stephens, *Annu. Rev. Phys. Chem.* **1974**, *25*, 201–232.
- [9] a) H. Solheim, K. Ruud, S. Coriani, P. Norman, *J. Phys. Chem. A* **2008**, *112*, 9615–9618; b) H. Solheim, K. Ruud, S. Coriani, P. Norman, *J. Chem. Phys.* **2008**, *128*, 094103; c) T. Kjaergaard, S. Coriani, K. Ruud, *Wiley Interdiscip. Rev. Comput. Mol. Sci.* **2012**, *2*, 443–455; d) M. Seth, M. Krykunov, T. Ziegler, J. Autschbach, A. Banerjee, *J. Chem. Phys.* **2008**, *128*, 144105; e) M. Seth, M. Krykunov, T. Ziegler, J. Autschbach, *J. Chem. Phys.* **2008**, *128*, 234102; f) M. Seth, J. Autschbach, T. Ziegler, *J. Chem. Theory Comput.* **2007**, *3*, 434–447; g) M. Krykunov, M. Seth, T. Ziegler, J. Autschbach, *J. Chem. Phys.* **2007**, *127*, 244102; h) P. Štěpánek, P. Bouř, *J. Comput. Chem.* **2013**, *34*, 1531–1539; i) K. M. Lee, K. Yabana, G. F. Bertsch, *J. Chem. Phys.* **2011**, *134*, 144106.
- [10] a) V. Andrushchenko, D. Padula, E. Zhivotova, S. Yamamoto, P. Bouř, *Chirality* **2014**, *26*, 655–662; b) P. Štěpánek, M. Straka, V. Andrushchenko, P. Bouř, *J. Chem. Phys.* **2013**, *138*, 151103; c) E. I. Solomon, K. M. Light, L. V. Liu, M. Srnc, S. D. Wong, *Acc. Chem. Res.* **2013**, *46*, 2725–2739; d) N. Lin, H. Solheim, X. Zhao, F. Santoro, K. Ruud, *J. Chem. Theory Comput.* **2013**, *9*, 1557–1567; e) P. Štěpánek, V. Andrushchenko, K. Ruud, P. Bouř, *J. Phys. Chem. A* **2012**, *116*, 778–783; f) M. Seth, T. Ziegler in *Advances in Inorganic Chemistry Vol. 62* (Eds.: R. VanEldik, J. Harley), Elsevier Academic Press, Inc., San Diego, **2010**, pp. 41–109; g) E. Hernandez-Marin, M. Seth, T. Ziegler, *Inorg. Chem.* **2010**, *49*, 6066–6076; h) G. A. Peralta, M. Seth, H. Zhekova, T. Ziegler, *Inorg. Chem.* **2008**, *47*, 4185–4198; i) M. Seth, T. Ziegler, J. Autschbach, *J. Chem. Phys.* **2005**, *122*, 094112.
- [11] A. V. Nemukhin, I. A. Topol, S. K. Burt, *J. Chem. Theory Comput.* **2006**, *2*, 292–299.
- [12] R. Send, V. R. I. Kaila, D. Sundholm, *J. Chem. Phys.* **2011**, *134*, 214114.
- [13] V. R. I. Kaila, R. Send, D. Sundholm, *Phys. Chem. Chem. Phys.* **2013**, *15*, 4491–4495.
- [14] C. Filippi, F. Buda, L. Guidoni, A. Sinicropi, *J. Chem. Theory Comput.* **2012**, *8*, 112–124.
- [15] M. T. P. Beerepoot, A. H. Steindal, K. Ruud, J. M. H. Olsen, *Comput. Theor. Chem.* **2014**, *1040*, 304–311.
- [16] T. Schwabe, M. T. P. Beerepoot, J. M. H. Olsen, J. Kongsted, *Phys. Chem. Chem. Phys.* **2015**, *17*, 2582–2588.
- [17] M. T. P. Beerepoot, A. H. S. Steindal, J. Kongsted, B. O. Brandsdal, L. Frediani, K. Ruud, J. M. H. Olsen, *Phys. Chem. Chem. Phys.* **2013**, *15*, 4735–4743.
- [18] M. T. P. Beerepoot, D. H. Friese, K. Ruud, *Phys. Chem. Chem. Phys.* **2014**, *16*, 5958–5964.
- [19] a) R. Gnanasekaran, *Chem. Phys. Lett.* **2013**, *587*, 61–67; b) Y. Xu, R. Gnanasekaran, D. M. Leitner, *Chem. Phys. Lett.* **2013**, *564*, 78–82.
- [20] a) R. Nifosi, P. Amat, V. Tozzini, *J. Comput. Chem.* **2007**, *28*, 2366–2377; b) E. Epifanovsky, I. Polyakov, B. Grigorenko, A. Nemukhin, A. I. Krylov, *J. Chem. Theory Comput.* **2009**, *5*, 1895–1906; c) C. Filippi, M. Zaccheddu, F. Buda, *J. Chem. Theory Comput.* **2009**, *5*, 2074–2087; d) H. M. List, J. M. Olsen, T. R. Rinza, O. Christiansen, J. Kongsted, *Int. J. Quantum Chem.* **2012**, *112*, 789–800.
- [21] M. A. L. Marques, X. López, D. Varsano, A. Castro, A. Rubio, *Phys. Rev. Lett.* **2003**, *90*, 258101.
- [22] P. Štěpánek, P. Bouř, *J. Comput. Chem.* **2015**, *36*, 723–730.
- [23] P. Štěpánek, M. Straka, J. Šebestík, P. Bouř, *Chem. Phys. Lett.* **2016**, *647*, 117–121.
- [24] T. Fahleson, J. Kauczor, P. Norman, F. Santoro, R. Improta, S. Coriani, *J. Phys. Chem. A* **2015**, *119*, 5476–5489.
- [25] S. Kojima, H. Ohkawa, T. Hirano, S. Maki, H. Niwa, M. Ohashi, S. Inouye, F. I. Tsuji, *Tetrahedron Lett.* **1998**, *39*, 5239–5242.
- [26] D. Padula, D. Picconi, A. Lami, G. Pescitelli, F. Santoro, *J. Phys. Chem. A* **2013**, *117*, 3355–3368.
- [27] J. Michl, *Tetrahedron* **1984**, *40*, 3845–3934.
- [28] A. D. Becke, *J. Chem. Phys.* **1993**, *98*, 5648–5652.
- [29] Y. Zhao, D. G. Truhlar, *Theor. Chem. Acc.* **2008**, *120*, 215–241.
- [30] T. Yanai, D. Tew, N. C. Handy, *Chem. Phys. Lett.* **2004**, *393*, 51–57.
- [31] J. P. Perdew, *Phys. Rev. B* **1986**, *33*, 8822–8824.

- [32] A. D. Laurent, D. Jacquemin, *Int. J. Quantum Chem.* **2013**, *113*, 2019–2039.
- [33] P. Štěpánek, P. Bouř, *Phys. Chem. Chem. Phys.* **2014**, *16*, 20639–20649.
- [34] J. Dong, K. M. Solntsev, L. M. Tolbert, *J. Am. Chem. Soc.* **2006**, *128*, 12038–12039.
- [35] Gaussian 09 (Revision D.01), M. J. Frisch, G. W. Trucks, H. B. Schlegel, G. E. Scuseria, M. A. Robb, J. R. Cheeseman, G. Scalmani, V. Barone, B. Mennucci, G. A. Petersson, H. Nakatsuji, M. Caricato, X. Li, H. P. Hratchian, A. F. Izmaylov, J. Bloino, G. Zheng, J. L. Sonnenberg, M. Hada, M. Ehara, K. Toyota, R. Fukuda, J. Hasegawa, M. Ishida, T. Nakajima, Y. Honda, O. Kitao, H. Nakai, T. Vreven, J. Montgomery, J. A., J. E. Peralta, F. Ogliaro, M. Bearpark, J. J. Heyd, E. Brothers, K. N. Kudin, V. N. Staroverov, R. Kobayashi, J. Normand, K. Raghavachari, A. Rendell, J. C. Burant, S. S. Iyengar, J. Tomasi, M. Cossi, N. Rega, J. M. Millam, M. Klene, J. E. Knox, J. B. Cross, V. Bakken, C. Adamo, J. Jaramillo, R. Gomperts, R. E. Stratmann, O. Yazyev, A. J. Austin, R. Cammi, C. Pomelli, J. W. Ochterski, R. L. Martin, K. Morokuma, V. G. Zakrzewski, G. A. Voth, P. Salvador, J. J. Dannenberg, S. Dapprich, A. D. Daniels, O. Farkas, J. B. Foresman, J. V. Ortiz, J. Cioslowski, D. J. Fox, Gaussian, Inc., Wallingford CT, **2009**.
- [36] A. Klamt in *The Encyclopedia of Computational Chemistry, Vol. 1* (Eds.: P. R. Schleyer, N. L. Allinger, T. Clark, J. Gasteiger, P. A. Kollman, H. F. Schaefer III, P. R. Schreiner), John Wiley & Sons, Chichester, **1998**, pp. 604–615.
- [37] F. Furche, R. Ahlrichs, *J. Chem. Phys.* **2002**, *117*, 7433–7447.

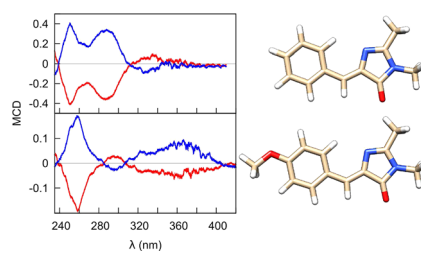
Manuscript received: March 27, 2016
 Accepted Article published: April 28, 2016
 Final Article published: ■ ■ ■, 2016

ARTICLES

P. Štěpánek, T. Y. Cowie, M. Šafařík,
J. Šebestík, R. Pohl, P. Bouř*



Resolving Electronic Transitions in Synthetic Fluorescent Protein Chromophores by Magnetic Circular Dichroism



Better understanding: Magnetic circular dichroism for a series of fluorescent protein chromophore derivatives provides specific spectral patterns, and in connection with density functional theory simulations it can be used for rational design of fluorescent probes.